International Soil and Water Conservation Research 12 (2024) 217–226

Contents lists available at ScienceDirect

International Soil and Water Conservation Research

journal homepage: www.elsevier.com/locate/iswcr

Original Research Article

Semi-automated detection of rangeland runoff and erosion control berms using high-resolution topography data

Li Li [a, b, c, *]

[a] Changjiang River Scientific Research Institute of Changjiang Water Resources Commission, Wuhan, 430010, China
[b] Research Center on Mountain Torrent & Geologic Disaster Prevention, Ministry of Water Resources, Wuhan, 430010, China
[c] University of Arizona, School of Natural Resources and the Environment, Tucson, AZ, 85719, USA

ARTICLE INFO

Article history:
Received 27 January 2023
Received in revised form
11 May 2023
Accepted 19 May 2023
Available online 4 June 2023

Keywords:
Earthen berm
Rangeland
Grayscale morphological reconstruction
Geomorphon
LiDAR

ABSTRACT

An inventory of topographic modifications is essential to addressing their impacts on hydrological and morphological processes in human-altered watersheds. However, such inventories are generally lacking. This study presents two workflows for semi-automatic detection of linear earthen runoff and erosion control berms in rangelands using high-resolution topographic data. The workflows consist of initial object identification by applying either morphological grayscale reconstruction (MGR) or the Geomorphon (GEO) method, followed by identification refinements through filters based on objects' horizontal and vertical information. Three sites were selected within the Altar Valley, Arizona, in the southwestern United States. One site was used for developing workflows and optimizing filter thresholds, and the other two sites were used to validate workflows. The results showed that: 1) The MGR-based workflow methodology could produce final precision and detection rates of up to 92% and 75%, respectively, and take less than 5 s for a 10.1 km^2 site; 2) The workflow based on the MGR method yielded greater identification accuracy than did the GEO workflow; 3) Object length, orientation, and eccentricity were important characteristics for identifying earthen berms, and are sensitive to general channel flow direction and berm shape; 4) Manual interrogation of topographic data and imagery can significantly improve identification precision rates. The proposed workflows will be useful for developing inventories of runoff and erosion control structures in support of sustainable rangeland management.

1. Introduction

Physical structures to manipulate surface runoff, mitigate land deterioration, and improve vegetation production have been used for thousands of years, with some ancient control structures still functioning today (Deng et al., 2021; Nichols & Degginger, 2021; Nichols et al., 2018, 2021; Stavi et al., 2020; Steinfeld et al., 2013). Across western United States rangelands, overgrazing in combination with recurrent droughts and floods have historically caused rangeland deterioration and other environmental problems (Dettenmaier et al., 2017; Havstad et al., 2015, pp. 75–93). In response, physical conservation works of various types, materials, and shapes have been constructed to manipulate surface runoff for managing water resources and for abating erosion problems (Nichols et al., 2021).

Typical physical structures include linear earthen water spreader berms, porous and non-porous check dams, and earthen stock tanks (Polyakov et al., 2014; Stavi et al., 2020). Earthen spreader berms built on hillslopes can play an important role in restoration of degraded rangelands (Fig. 1, Nichols et al., 2021). As summarized by Stavi et al. (2020), earthen berms can retain water on-site to promote vegetation growth on hillslopes (as shown in Fig. 1), which is of importance in rangelands where water is scarce. The increased vegetative cover subsequently promotes geo-ecological feedbacks, such as improved soil quality and reduced soil erosion. Moreover, earthen berms can facilitate on-site deposition of mineral and organic matter, which are also beneficial for ecosystem functioning.

However, the construction of earthen berms also raises some

* Changjiang River Scientific Research Institute of Changjiang Water Resources Commission, Wuhan, 430010, China.
E-mail address: liliazacademy@outlook.com.

https://doi.org/10.1016/j.iswcr.2023.05.004

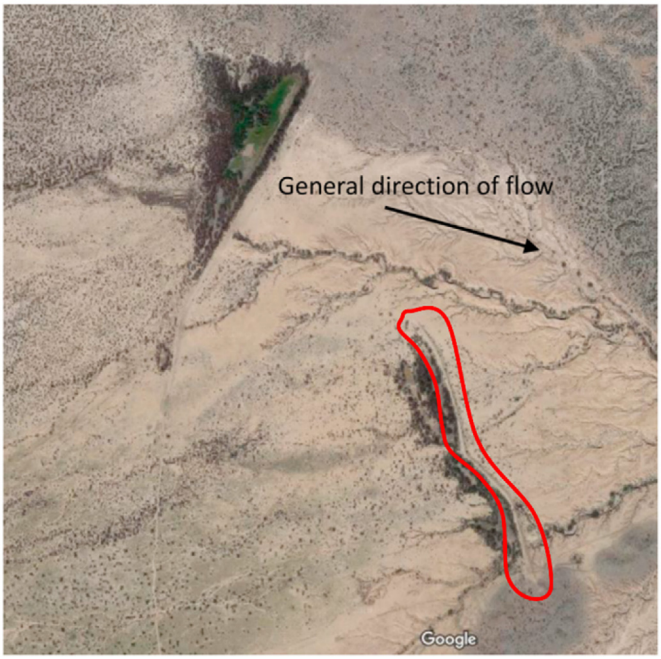

Fig. 1. Water spreader berm (bounded by red line) and vegetation on the upslope side of water spreader berms. Picture was sourced from Nichols et al. (2021).

concerns. Failures or unwanted consequences of the earthen berms have been previously reported (Nichols et al., 2018; Peterson & Branson, 1962; Stavi et al., 2018, 2019). Nichols and Degginger (2021) documented that 15% of 667 shorter water spreader berms that were built during the past several decades in the Altar Valley in the southwestern US have been breached and 29% have experienced lateral scour, causing geomorphic impacts and imposing significant environmental threats to rangeland productivity. In addition, deposited sediment on the upslope side of berms creates topographically higher areas. Runoff then can bypass the berms with greater erosive power and transport capacity, enhancing both hydrologic and sediment connectivity downslope. Moreover, disturbance of the uppermost layers of soil by heavy machinery during berm construction is likely to decrease natural geodiversity and increase hydrological connectivity, resulting in higher erosion rates (Stavi et al., 2020). It is therefore critical to investigate the impacts and conditions of earthen berms, especially unmaintained ones, to better understand the response of hydrologic, vegetation, geomorphologic, and landscape evolution processes, as well as to guide future land management decisions. An inventory of earthen berms in rangelands is a fundamental first step. However, such inventories are rare, and to date, database development has relied on time-consuming field visits and digitization of the conservation structures from aerial images supplemented with topographic data (Nichols & Degginger, 2021; Nichols et al., 2021).

As high-resolution LiDAR-derived Digital Elevation Models (DEMs) become more accessible, identifying objects, including natural geomorphic features and human-made earthworks, becomes more feasible (Tarolli, 2014; Tarolli et al., 2012). For example, McKean and Roering (2004) used statistical, Laplacian, and spectral analyses to quantify the local surface roughness of high-resolution DEMs, and then used the spatial patterns of the surface roughness to detect and map landslide areas. Tarolli et al. (2012) calculated landform curvature at different spatial scales and statistically analyzed curvature variability to determine the optimal statistical thresholds for distinguishing shallow landslides in the Eastern Italian Alps. Cazorzi et al. (2013) analyzed surface topographic attributes, including slope gradient, terrain curvature, and entropy, to detect drainage networks in two typical alluvial-plain areas in the Northeastern Italy. Sărășan et al. (2019) used Geomorphon maps and Wetness Index maps, with the aid of image segmentation processing, to map drumlins in southeastern Germany. In general, the above-cited studies calculated terrain attributes from high-resolution DEMs and, by analyzing the distribution of those attributes, statistically defined thresholds were determined and used to objectively distinguish the geomorphic features and objects. In these studies, the targeted features and objects were relatively large and obvious as compared to other surface features, hence a single terrain attribute and associated threshold usually were effective for identifying them.

There have been few attempts made to identify human-made earthen conservation structures in rangelands from DEMs, in part because high-resolution topographic data sufficient to describe such structures are lacking for many of these landscapes. Even where such data are available, there are several challenges to automating procedures for identifying runoff and erosion control structures including: 1) In contrast to high-relief mountainous areas, it can be difficult to distinguish landform features (e.g., summit, shoulder, and valley) in areas where topography is relatively low-relief (Tucker et al., 2001); 2) Compared to geomorphic features such as drainage channels, terraces, and drumlins, typical rangeland runoff and erosion control structures are irregularly distributed, are relatively small (Nichols & Degginger, 2021), and usually are not the dominant topographic feature. Thus, it is challenging to distinguish them from other random surface irregularities; 3) Many rangeland runoff and erosion control structures were made without technical standards, thus there is little to no documentations. Even if such records existed, the present-day form and condition of earthen berms may not be as originally designed due to erosion. These challenges make defining the terrain attribute thresholds needed to detect physical structures, such as earthen berms, difficult in rangeland landscapes.

Steinfeld et al. (2013) proposed a workflow based on DEM analysis to detect floodplain earthworks. In their work, two iterations of surface filters in combination with removing natural channels were used to generate a surface that only included the natural landscape undulations while excluded local earthwork relief. Pixels exceeding ±0.1 m elevation difference compared to adjacent pixels in the generated surface were searched and aggregated into polygons. A further analysis of polygon compactness index, height, and vertices was conducted to develop probability regression models for classifying different types of earthworks. The result was detection of floodplain earthworks, including levees and tanks, from topographic data. Their study suggested that automated detection of human-made earthworks in low-relief landscapes (i.e., floodplains) may require more effort to analyze the identified object shape and height, rather than solely using a single terrain attribute threshold. It should be noted that the earthworks identified in the study of Steinfeld et al. (2013) were the dominant features in images, while typical earthen berms in southwestern US rangelands are of various dimensions, the non-dominant landscape features, and are more irregularly distributed across the landscape.

The objective of this work is to develop and test semi-automated methods for identifying linear earthen berms using high-resolution (1-m) DEMs. We hypothesize that the detection accuracy and rate of typical rangeland runoff and erosion control berms would be improved by assessing object shape and height characteristics. Extracting such features will be useful for developing inventories of runoff and erosion control structures in support of sustainable rangeland management.

2. Methods

2.1. Study area

The study area is located in the Altar Valley, Arizona in the western North American Basin and Range Physiographic Province (Fig. 2). This semi-arid basin is bounded by the Sierrita, Cerro Colorado, Las Guijas, Baboquivari, and Coyote mountains. Annual precipitation is approximately 415 mm, of which more than half occurs during the North American Monsoon from July to September. The valley is underlain by alluvial fill to a depth up to 600 m and is comprised of silt, sand, and gravel, which are coarse and permeable. Compared to the historic landscapes in the Altar Valley wherein runoff could spread laterally, incising tributary channels are common and connected to the larger entrenched Altar Wash. This connected channel network facilitates the high-velocity flow that is generated in the monsoon season, which further enhances channel incision and bank erosion (Nichols & Degginger, 2021). For several decades in the 1900s, the topography of the Altar Valley was altered to capture surface runoff and mitigate erosion through construction of earthen berms. Various types of manmade structures, including check dams, runoff control structures, short earthen spurs, stock tanks, and road features were intentionally constructed to offer conservation benefits in the valley, and all those structures have caused topographic alterations (Nichols & Degginger, 2021).

Three sites selected within the Altar Valley study area (A, B, and C) are located on the west side of the Altar Wash, with areas (km^2)

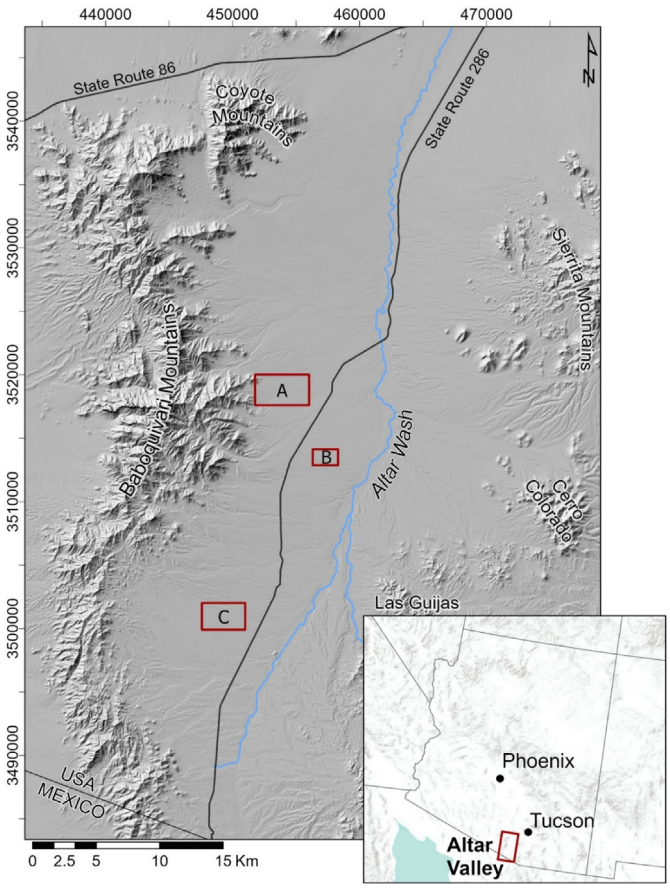

Fig. 2. Altar Valley and the three research sites (Site A for developing workflows and for optimizing thresholds and parameters, Sites B and C for validations of the workflows).

of 10.1 for Site A, 2.4 for Site B, and 7.1 for Site C (Fig. 2). In this study, we limited the identification of features to linear earthen berms that were constructed to control surface runoff and erosion within the selected sites. This study does not attempt to identify stock tanks or lateral channel berms. Aerial LiDAR data sourced from the Pima Country Regional Flood Control District (July 9–14, 2016) was used to create a 1-m DEM for the Altar Valley in a previous study (Nichols & Degginger, 2021). Reference berms were manually identified and digitized as line features in ArcGIS Pro using aerial imagery and hillshade 3D representations of the landscape surface developed from DEMs (Nichols & Degginger, 2021). These reference berms were used in the current study to support workflow development.

2.2. Proposed workflows

In the present study, we proposed two workflows as shown in Fig. 3. The general idea of the two workflows is to conduct initial berm identification first, and then to refine the identification using multiple filters relating berm horizontal and vertical information. The first workflow used morphological grayscale reconstruction method to conduct initial identification (Fig. 3a), and the second workflow used the Geomorphon method to conduct initial identification (Fig. 3b). More details regarding the two workflows were described as follows.

2.2.1. Initial berm identification

The most conspicuous feature of an earthen berm in comparison with the surrounding areas (pixels), is its relatively higher elevation. Two approaches, morphological grayscale reconstruction (Fig. 3a) and the Geomorphon method (Fig. 3b), were separately used to conduct initial berm identification. The set of resultant potential berms were refined using feature threshold-based filters, and the precision and accuracy of the final identifications were compared.

2.2.1.1. Morphological grayscale reconstruction method (MGR). Morphological grayscale reconstruction is a process where the marker image (Y) is repeatedly dilated, and the dilated image (Y^*) is always lying underneath the mask image (X), until the dilated image (Y^*) reaches stability and its contour fits under the mask image (X) (Vincent, 1993), and the peaks in the marker image spread out (Fig. 4).

The mathematical expression of the repeated dilation processes is given by Vincent (1993) as:

$$R = \rho_X(Y) = \delta_X^{(n)}(Y) = \delta_X^{(1)}(Y) \circ \delta_X^{(1)}(Y) \circ \ldots \delta_X^{(1)}(Y) \quad (1)$$

where $\rho_X(Y)$ is the reconstructed X from Y, by performing n successive geodesic dilation of size 1 ($\delta_X^{(1)}(Y)$).

$$\delta_X^{(1)}(Y) = \delta(Y) \wedge X \quad (2)$$

where $\wedge$ stands for the pointwise minimum, and $\delta(Y)$ is the basic dilation of Y.

Any given DEM can be considered as a grayscale image wherein each pixel has three dimensions. Dimensions x and y represent pixel position, and dimension z represents the intensity of the pixel (x, y); z is interchangeable with the elevation value of a pixel as in a DEM. We used morphological grayscale reconstruction to create a filtered ideal DEM to remove elevation noise while retaining the dominant elevation features (i.e., the global trend of landscape undulations). In the present study, morphological grayscale reconstruction was implemented using the Image Processing

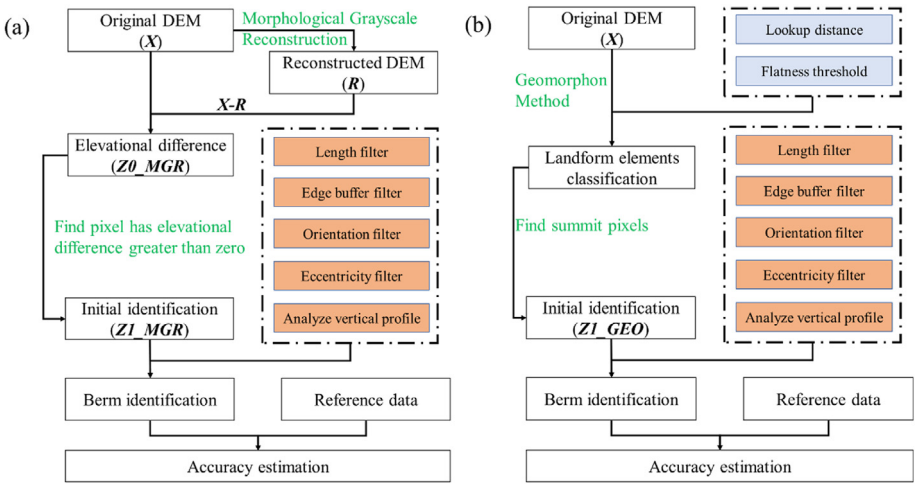

Fig. 3. The proposed workflows that one is based on morphological grayscale reconstruction method (a) and that the other one is based on the Geomorphon method (b).

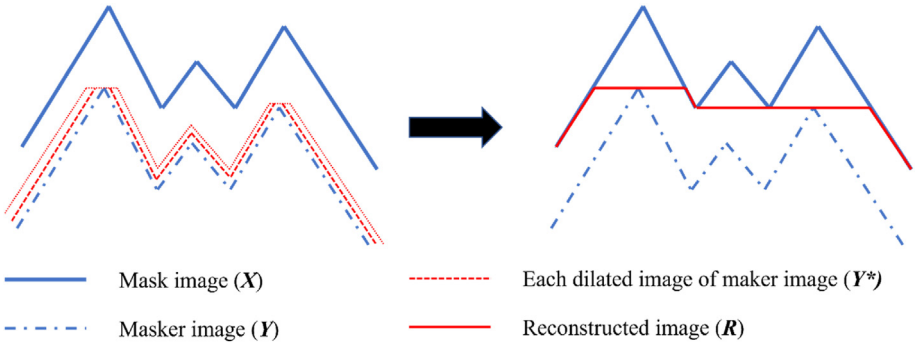

Fig. 4. A schematic example of Morphological grayscale reconstruction procedures.

Toolbox within MATLAB (MATLAB 2021a). Analysis of DEMs was accomplished using the TopoToolbox add-on for MATLAB (Schwanghart & Kuhn, 2010).

Mask image (X): To maximize the search for potential local peak areas on the landscape, the mask image, X, which was the original DEM without application of a smoothing filter, was used. This is a critical step because the features of small earthen berms are likely to be eliminated if a smoothing filter is applied.

Maker image (Y): A common way to generate a marker image, Y, is by subtracting a constant shift value from the mask image. However, the reconstruction result will be significantly affected by the selection of the constant shift value (Arefi & Hahn, 2012), thus presenting a challenge for identifying earthen berms with wide spectrum of heights. In this study, a marker image was achieved by eroding the mask image using a morphological structuring disk, such that, the high-intensity objects in the mask image were highlighted in the marker image. A rough measurement of a subset of reference earthen berms showed that the base width of earth berms ranged from 3 to 10 m. Hence, a radius of 7 m was selected for creating a morphological structuring disk.

Initial berm identification: The elevational difference, *Z0_MGR*, between the original DEM and its reconstructed image (R) were calculated:

$$Z0\_MGR = X - \rho_X(Y) = X - R \tag{3}$$

Then, an elevation threshold was applied to the *Z0_MGR* to differentiate ground and above-ground pixels. Those pixels in the *Z0_MGR* that have intensity values greater than zero were considered to be above-ground points, and were assigned a new value of 1 to produce an image *Z1_MGR*. The resultant output of this initial identification of earthen berms, *Z1_MGR*, was thus comprised of only those above-ground pixels with a constant intensity value of 1.

2.2.1.2. Geomorphon method (GEO). The Geomorphon method is an approach to classify landforms proposed by Jasiewicz and Stepinski (2013) based on the ternary pattern of DEM pixels. To determine the ternary pattern of each pixel, traditionally the elevation difference between the pixel and its neighboring pixels in a moving window (3 pixels by 3 pixels) is quantified. While the Geomorphon method determines the ternary pattern of each pixel by comparing the zenith angle and nadir angle of a profile starting from the pixel and extending a lookup distance (L) along the principal directions. The difference between the zenith angle and nadir angle is further compared to a flatness threshold (t) to determine the value of each slot of a ternary pattern. By analyzing the ternary pattern using the eight slot values along eight principal directions, each pixel of the DEM can be classified into one of the ten common landform elements: flat, peak, ridge, shoulder, spur, slope, pit, valley, footslope, and hollow (Jasiewicz & Stepinski, 2013). The Geomorphon method is currently incorporated into GRASS-GIS (GRASS Development Team, 2017) and SAGA-GIS (Conrad et al., 2015), both of which are open-source software packages. Note here, the category of "peak" in the pioneering study of Jasiewicz and Stepinski (2013) is termed as "summit" in both GRASS-GIS and SAGA-GIS.

By running SAGA-GIS using several combinations of lookup

distance and flatness threshold, and through an overlay analysis of the resultant Geomorphon map and the earthen berm referenced polygons, both ridge and summit pixels were found to be useful for extracting earthen berms. The overlay analysis results can be found in Supplement Section 1. The results of extracting ridge pixels, however, included a substantial number of false-positive identifications, posing challenges for further refinement of the identification results. Therefore, the extractions of the summit pixels alone were used as the initial identification result, *Z1_GEO*. It was observed that the summit pixels were often connected as a very thin shape likely because for each berm, only the top rather than the whole based of the berm, was classified as "summit". To address this, objects in image, *Z1_GEO*, were grown using a small moving window (2 pixels) and 2D convolution function in MATLAB, so that the identified objects in the image, *Z1_GEO*, would have a width of at least 5 pixels (m); this is a more realistic representation of berm widths in comparison to measurements from aerial imagery.

Landform classification results are affected by the two input parameters - lookup distance (L) and flatness threshold (t) (Jasiewicz & Stepinski, 2013; Sărăș;an et al., 2019). Therefore, it is of critical importance to select optimal parameter values to successfully identify relatively small landscape elements. However, there is no guidance regarding how to objectively select these optimal parameters. Jasiewicz and Stepinski (2013) suggested that "*the optimal value of L should be large enough to map landforms at most relevant scales but small enough for rapid computations*" and that "*the value of L determines the maximum scale at which we can find the landform elements*". Hence, in the example case of Jasiewicz and Stepinski (2013, Fig. 8 in their study), multiple L and t values were tested until optimal values were determined to successfully map a particular type of landscape. In our study, a series of lookup distance values ranging from 10 to 100 m, and flatness thresholds ranging from 0 to 1°, were tested to optimize these two parameters by comparing their identification rate and accuracy. The tested lookup distances are larger than the width of the earthen berms but are relatively smaller than the length of the berms, and the tested flatness thresholds were in the value range of previous studies.

2.2.2. Refining berm identification

After the initial identification, threshold filters incorporating horizontal and vertical information were developed and applied using MATLAB to improve the rate and precision of berm detection. A total of four additional threshold filters were applied following the initial identification to eliminate those objects that were not actually berms, i.e., false-positive features. The filters were applied independently to the output of the initial identifications of both the morphological reconstruction method (*Z1_MGR*) and the Geomorphon method (*Z1_GEO*).

2.2.2.1. Refining identifications by applying horizontal information. Length filter: The first filter implemented removed objects based on length. Objects having a major-axis length less than a specified maximum length were removed to eliminate both scattered pixels and less-connected identified objects. The optimal value of the length threshold is large enough to maximize the removal of scattered objects and also small enough to maximize the search of true earthen berms.

Edge buffer filter: The second filter applied removed scattered pixels that touched the edge of the image. During image processing and initial berm identification, some scattered pixels near the edges of the image were enlarged and consequently formed unwanted objects that touched the edge of the image when convolution and dilation algorithms were implemented. To remove those objects, a filter consisting of a buffer from the outer edges of the image was created, so that, objects located within a specified buffer width were filtered out. The remaining objects in the buffered image then were smoothed using a small moving window (3 pixels) to obtain more rounded outer boundaries, which facilitated subsequent steps to analyze vertical elevation profiles, filled holes inside objects, and connected very close isolated objects.

Orientation filter: The third filter removed objects that had small orientation angles as compared to the general flow direction. Earthen berms for water and erosion control tend to be built perpendicular to surface flow direction, such that their orientations relative to flow direction are relatively large. In other words, identified objects with small orientation angles compared to the general flow direction are less likely to be earthen berms. In any case of calculating orientation angle, a reference axis is required. In our case, the general flow direction was from west to east along the x-axis in the images (Fig. 2). Therefore, we defined west to east as the referenced flow direction. Orientation angle (i.e., $|\theta|$) between an identified object and this referenced flow direction consequently was computed for each identified object. We then set a threshold to the $|\theta|$ to remove objects with small orientation angle to the referenced flow direction.

One may argue orientation threshold would be better to be applied to the angle between each identified object and its corresponding upslope local flow direction, rather than the general flow direction. This is a compromise. Supposing the orientation angle between a corresponding upslope local flow direction and the referenced flow direction is β, therefore, the angle between each identified object and its corresponding upslope local flow direction could be calculated as $|\ \theta \pm \beta\ |$. However, β value is difficult to determine due to the large variations in direction of each channel segment. The reasons are twofold. On one hand, accurately extracting channel network with different channel orders involves more calculations, as well as producing uncertainties. On the other hand, the corresponding upslope local flow direction of each objects need to be located and somewhat smoothed, since local flow direction is not uniform but with toturosity. Therefore, we directly set orientation threshold to $|\theta|$, which is the orientation angle between an identified object and the referenced flow direction, rather than to $|\ \theta \pm \beta\ |$, which is the orientation angle between each identified object and its corresponding upslope local flow direction.

Eccentricity filter: The fourth filter was implemented to filter out objects that had small eccentricity. Earthen berms tend to be linear segments, thus, objects that deviate from a circular shape are more likely to be berms. Eccentricity is defined as the ratio of the distance of the two focus points of the fitted ellipse of the object to the major axis length of the fitted ellipse. The value of eccentricity of objects usually ranges from 0 to 1, and as eccentricity increases the objects are more linear.

In the identification procedures, we applied the length and edge buffer first to remove as much as possible unwanted objects. Therefore, few efforts will be taken to calculate the orientation and eccentricity of the remaining objects. The eccentricity and orientation filters can be used either simultaneously or in succession.

2.2.2.2. Refining berm identification by analyzing vertical elevation profiles. The application of the abovementioned four filters, which focused on object horizontal characteristics, reduced the number of potential berms (e.g., 223,592 at Site A) to dozens of isolated, connected objects. Because berms have a characteristic cross-sectional shape, analysis of the vertical elevation profiles of the remaining isolated objects helped to evaluate their cross-sectional shape to determine if they were characteristic of a typical earth berm (Fig. 5). The vertical elevation profile of a cross section through an object was obtained by drawing a straight line perpendicular to the object through the object's center. The peak, upslope, and downslope points were then determined for each

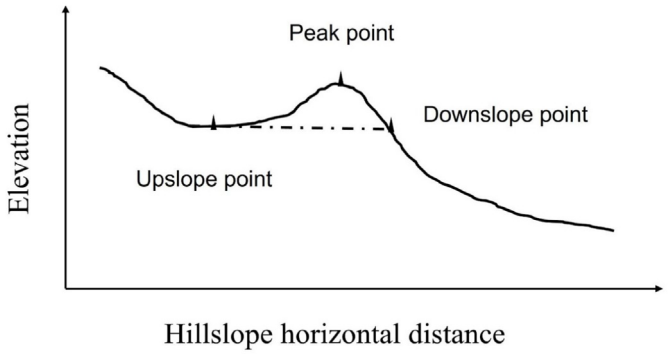

Fig. 5. A schematic example of a typical earthen berm located on a hillslope.

vertical elevation profile. We made a rule for each identified object after the application of the abovementioned four filters that, the elevation of the peak point of each identified object should be greater than the averaged elevation of the upslope and downslope points of the profile. If the identified object did not follow this rule, the object was removed. We made this rule to ensure that the peak of the identified object was relatively higher to ensure exclusion of misclassified features located in large depressions (for example, a local topographic higher area within a channel) rather than on the hillslope.

2.3. Accuracy assessment

The accuracy of earthen berm identification was assessed by evaluating the detection precision and rate in comparison to the manually derived reference berms. Each identified object was classified into one of the following three categories: (1) true-positive (TP), an object that matches the reference data and is actually a berm; (2) true-negative (TN), a referenced berm that is not found using the proposed workflows; (3) false-positive (FP), an identified object using the proposed workflow that is not in the reference dataset. Two mathematical indices, precision rate and detection rate, were used to quantify the accuracy of identification results (Sărăș;an et al., 2019). Accuracy was calculated using the identification result after each threshold filter to evaluate the performance of the automated proportion of the proposed workflow.

$$precision\ (PC) = \frac{TP}{TP + FP} \tag{4}$$

$$detection\ rate\ (DT) = \frac{TP}{TP + TN} \tag{5}$$

3. Results

3.1. Filter threshold calibrations

3.1.1. Identification based on the morphological grayscale reconstruction (MGR) method

The following describes the results of optimizing and determining filter values for Site A based on initial identification using the MGR method. The MGR method initially identified in total of 223,592 features, which include connected objects, less-connected objects, and scattered points. After applying the optimal filter values in succession, the estimated precision rate and detection rates of 82% and 77% were achieved (Table 1). Figures showing results after applying each optimized filter are available in Supplement Section 2.

Rough measurements of a subset of reference earthen berms showed that the minimum berm length was approximately 25 m. Therefore, identified objects were filtered at 1m increments from values ranging from 15 to 24 m for the object length threshold. The use of a minimum object length value less than 25 m maximized identification of those berms that appeared with two segments in the DEM; on the ground, it is common for berms to be breached, resulting in a single berm being represented as two or more separate segments. It was determined that the optimal object length threshold was 17 m.

An edge buffer filter width of 50 m was used to remove scattered objects near the edges of the image. The buffer width value of 50 m can be adjusted by manually investigating the spatial distribution of those near-edge objects, to ensure that true berms are not removed by the buffer.

Among the 53 reference berms at Site A, 50 berms (94%) had an orientation angle, $|\theta|$, greater than 25°. The optimal orientation angle, which removed objects with a small orientation angle as compared to the general flow direction, was determined by testing values from 18 to 24° at increments of 1°. The optimal orientation angle filter was found to be 21°.

Among the 53 referenced berms at Site A, 50 berms (94%) have an eccentricity greater than 0.95. Therefore, eccentricity filter values ranging from 0.90 to 0.95 were evaluated at an increment of 0.1. Values greater than 0.95 were not considered because automatically identified objects had a generally more irregular shape as compared to the idealized shape of the manually digitized reference objects. The optimal object eccentricity threshold was 0.95.

3.1.2. Identification based on the Geomorphon (GEO) method

The following describes the results of optimizing and determining filter values for Site A based on the initial identification results from the GEO method. The GEO method was affected by the two parameters, lookup distance *(L)* and flatness threshold *(t)*, therefore, *L* and *t* were calibrated while using the optimized filter values in Table 1, although the buffer width was adjusted to the changing *L*. Optimized values of 100 and 0.1 were determined for *L* and *t*, respectively. The GEO method initially identified in total of 61,336 features, which included connected objects, less-connected objects, and scattered points. By using the optimal filter values, the calculated precision rate and detection rate were 69% and 68%, respectively (Table 2). Figures showing results after applying each optimized filter are available in Supplement Section 3.

3.2. Workflow validation

The above-described workflows and resultant optimized filter thresholds developed at Site A were applied to Sites B and C to independently test their application for identifying linear earthen berms.

3.2.1. Validation results at Site B

The identification accuracies at Site B based on the MGR method after applying each filter are presented in Table 3. The final precision and detection rates were 92% and 75%, respectively (also see Fig. 6). The workflow based on the GEO method yielded a 63% precision rate and an 83% detection rate at Site B (Table 4).

3.2.2. Validation at Site C

When the optimized filter thresholds developed at Site A were applied to Site C, the MGR workflow produced a 69% precision rate and a 59% detection rate. Because the eccentricity of the referenced berms of Site C was lower than that of Sites A and B, the object eccentricity threshold was adjusted from 0.95 to 0.93. In addition,

Table 1
Summary of filter values and achieved accuracies based on 223,592 potential berms identified using Morphological Grayscale Reconstruction at Site A in the Altar Valley, AZ. Number of berms in reference dataset = 53.

Procedures	Filter value	Count				Precision rate	detection rate
		Objects	TP[a]	FP[a]	TN[a]		
1. apply length filter	17 m	289	47	232	6	17%	89%
2. apply edge buffer filter	50 m	227	47	170	6	22%	89%
3. apply orientation filter	21°	83	45	33	8	58%	85%
4. apply eccentricity filter	0.95	55	41	10	12	80%	77%
5. analyze vertical profile		54	41	9	12	82%	77%

[a] TP stands for true-positive; TN stands for true-negative; FP stands for false-positive. Same for the following tables.

Table 2
Summary of filter values and achieved accuracies based on 61,336 potential berms identified using the Geomorphon method (lookup distance = 100m and flatness threshold = 0.1) at Site A in the Altar Valley, AZ. Number of berms in reference dataset = 53.

Procedures	Filter value	Count				Precision rate	Detection rate
		Objects	TP	FP	TN		
1. apply length filter	17 m	413	44	349	9	11%	83%
2. apply edge buffer filter	100 m	310	43	248	10	15%	81%
3. apply orientation filter	21°	87	36	47	17	43%	68%
4. apply eccentricity filter	0.95	59	36	19	17	65%	68%
5. analyze vertical profile		54	36	16	17	69%	68%

Table 3
Summary of filter values and achieved accuracies based on 110,895 potential berms identified using Morphological Grayscale Reconstruction at Site B in the Altar Valley, AZ. Number of berms in reference dataset = 16.

Procedures	Filter value	Count				Precision rate	Detection rate
		Objects	TP	FP	TN		
1. apply length filter	17 m	61	12	43	4	22%	75%
2. apply edge buffer filter	50 m	41	12	23	4	34%	75%
3. apply orientation filter	21°	21	12	5	4	71%	75%
4. apply eccentricity filter	0.95	17	12	1	4	92%	75%
5. analyze vertical profile		17	12	1	4	92%	75%

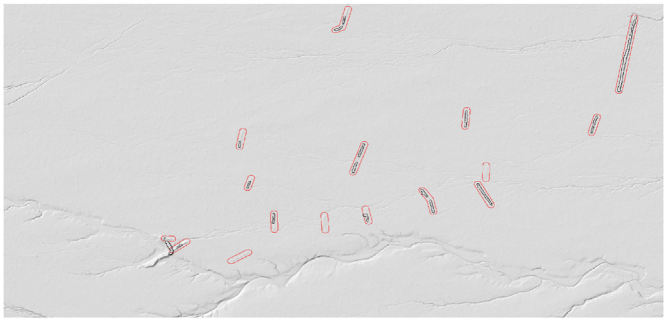

Fig. 6. The final identification results from the workflow based on the Morphological Grayscale Reconstruction method at Site B (red lines bound the referenced berms, and black lines bound the MGR identified berms).

several of the identified false positives (FPs) had orientations greater than 21°, we therefore increased the object orientation threshold from 21 to 25°. By adjusting those thresholds, the precision rate and detection rate were 60% and 73%, respectively (Table 5 and Fig. 7). Making these threshold adjustments did not improve the identification results based on the GEO method which resulted in a precision rate of 41% and detection rate of 44% (Table 6).

4. Discussion

Using earthen berms to harvest runoff and to mitigate soil erosion has a long history. Traditionally, attention has been paid to the watershed hydrological response, the spatiotemporal variations

Table 4
Summary of filter values and achieved accuracies based on 53,298 potential berms identified using the Geomorphon method (lookup distance = 100m and flatness threshold = 0.1) at Site B in the Altar Valley, AZ. Number of berms in reference dataset = 16.

Procedures	Filter value	Count				Precision rate	Detection rate
		Objects	TP	FP	TN		
1. apply length filter	17 m	86	13	59	3	18%	81%
2. apply edge buffer filter	100 m	48	13	22	3	37%	81%
3. apply orientation filter	21°	22	12	4	4	75%	75%
4. apply eccentricity filter	0.95	15	10	6	2	63%	83%
5. analyze vertical profile		15	10	6	2	63%	83%

Table 5
Summary of filter values and achieved accuracies based on 247,402 potential berms identified using Morphological Grayscale Reconstruction at Site B in the Altar Valley, AZ. Number of berms in reference dataset = 41.

Procedures	Filter value	Count				Precision rate	Detection rate
		Objects	TP	FP	TN		
1. apply length filter	17 m	258	47	232	6	17%	89%
2. apply edge buffer filter	100 m	203	37	154	4	19%	90%
3. apply orientation filter	25°	92	34	52	7	40%	83%
4. apply eccentricity filter	0.93	60	30	24	11	56%	73%
5. analyze vertical profile		48	30	20	11	60%	73%

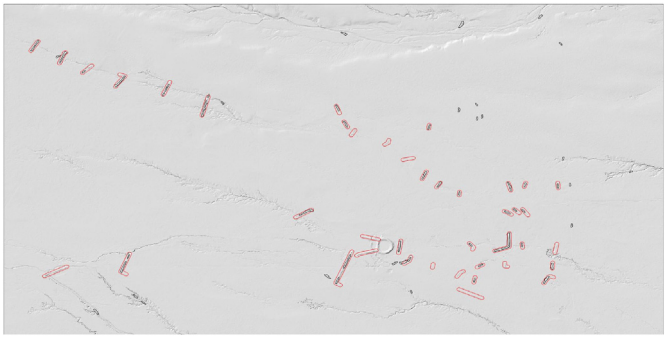

Fig. 7. The final identification results from the workflow based on the Morphological Grayscale Reconstruction method at Site C (red lines bound the referenced berms, and black lines bound the identified berms).

of runoff generation, sediment yield, soil moisture, and vegetation growth. Less attention has been given to the impacts of runoff and erosion mitigation structures on watershed morphology. The pioneering study of Nichols et al. (2018) documented that when these structures are not maintained, earthen berms can have substantial morphological impacts. For example, lateral scour caused by concentrated flow around a berm can increase erosion and incision. Locating these conservation structures in rangelands is essential to addressing their potential impacts. However, due to the limited availability of high-resolution topographic data and the irregular spatial arrangement of earthen berms across the landscape, such inventories are lacking. In this study, we proposed methods for identifying those isolated, irregularly distributed, and relatively small earthen berms by applying multiple filter workflows to high-resolution topographic data.

4.1. Benefits of using multiple filters

We hypothesized that the accuracy of detecting earthen berms in rangelands using semi-automatic methods would improve by assessing object shape and cross-sectional characteristics. This hypothesis was supported by the results presented in Tables 1–6 More than ten thousand objects were initially identified when applying either the MGR or the GEO methods with detection and precision rate increasing with the application of data filters. The validation results showed that the MGR-based workflow could produce final precision and detection rates of up to 92% and 75%, respectively. Given the fact that earthen berms accounted for less than 1% of the total DEM pixel count at the three study sites, our results suggest that earthen berms can be successfully detected using semi-automated workflows from high-resolution topographic data. Compared to previous studies in which a single terrain attribute threshold was used to identify objects (Cazorzi et al., 2013; Tarolli et al., 2012), the use of multiple filters in the present study furthers the possibility of successfully identifying the location and number of these relatively small, scattered features across the rangeland landscapes.

In addition to the filters presented in the methods of this study, we also tested slope, curvature, and entropy thresholds, and found that land surface irregularities located near channel banks caused problematic identification results when those thresholds were used (see Supplement Section 4). Land surface irregularities included features such as lateral channel bank protection berms, and other surface variations caused by abrupt changes both in elevation and slope gradients near hillslope-to-channel transitions (Nichols & Degginger, 2021). As documented by Nichols and Degginger (2021), more than 400 topographic alterations caused by gas pipeline construction were found within the Altar Valley. The use of a single terrain attribute threshold was insufficient to differentiate the earthen berms from those more conspicuous surface irregularities. Another concern is the issue of scale. A well-accepted concept in terrain and geomorphological analysis is that an optimal scale is required to accurately estimate the variability of terrain attributes (Tarolli, 2014). In our study, when a low-pass filter (small moving-window) was applied to a DEM, small-scale surface irregularities were preserved, including both the earthen berms and other topographic non-berm features, which required additional efforts to remove from consideration as berms. When a high-pass filter (large moving-window) was implemented, only large-scale surface features were preserved, and the smaller earthen berms were filtered out. Given the broad range of berm lengths and orientations, defining a single optimal scale that applies to variable terrain was difficult.

One may be concerned about the efficiency of the presented workflows with multiple filters. For the workflow based on MGR

Table 6
Summary of filter values and achieved accuracies based on 108,309 potential berms identified using the Geomorphon method (lookup distance = 100m and flatness threshold = 0.1) at Site B in the Altar Valley, AZ. Number of berms in reference dataset = 41.

Procedures	Filter value	Count				Precision rate	Detection rate
		Objects	TP	FP	TN		
1. apply length filter	17 m	444	25	397	16	6%	61%
2. apply edge buffer filter	100 m	240	25	193	16	11%	61%
3. apply orientation filter	25°	81	18	55	23	25%	44%
4. apply eccentricity filter	0.93	55	18	30	23	38%	44%
5. analyze vertical profile		41	18	26	23	41%	44%

method, all the codes were written and run at the MATLAB platform, the total running time of conducting initial identification and refinements is approximately 4.5 s for Site A (see Supplement Section 5). For the workflow based on GEO method, SAGA software was run first to get the Geomorphon output, and then the output was analyzed at the MATLAB platform, therefore, the total running time is several minutes longer.

4.2. The comparison between MGR- and GEO-based method

Both MGR and GEO method are used to conduct initial berm identification. The filters and recommended filter values are the same for each research site. In other words, those two workflows were compared under the same conditions. Overall, the workflow based on MGR yielded greater identification accuracy than did the GEO workflow. The reasons for those different identification results are twofold. On the one hand, the GEO method did not directly identify berms. We found that both ridge and summit pixels were useful for extracting earthen berm through overlay analysis. Although the ridge pixels did coincide with true berms, this pixel class also consisted of a substantial number of patches of non-earthen berm areas (e.g., natural hillslope ridge); therefore, only the extraction of summit pixels was used for initial identification (see Method section). In fact, we did not simply drop the ridge pixels. Except the overlay analysis that described in the method section, another test was conducted to use both ridge and summit pixels as initial identification, the final identification accuracy significantly decreased even using the same filter values (see Supplement Section 6). On the other hand, the pixel classification of ridge was affected by the lookup distance and flatness thresholds. In the present study, a series of lookup distance values ranging from 10 to 100 m, and multiple flatness thresholds ranging from 0 to 1°, were tested and it was determined that those two parameters significantly affected the identification and precision rates (Jasiewicz & Stepinski, 2013).

Even though both the lookup distance and flatness thresholds were optimized in the present study, we believed the workflow based on the Geomorphon method could be improved if more efforts are devoted to exploiting other Geomorphon output/input parameters. Nevertheless, the present study suggested that using Geomorphon method first and then applying multiple filters is feasible to identify dozens of small and isolated objects from half million DEM pixels.

4.3. The comparison of different filters

The object length and orientation filters were more important for removing misidentifications than other filters (Tables 1–6). The length filter successfully removed isolated pixels and less-connected objects. Conceptually, an optimal length threshold should be large enough to maximize the removal of scattered objects while also maximizing the search of true earthen berms. The optimized length threshold was determined to be 17 m, which was in the range of berm lengths measured in the reference data (Nichols et al., 2021), but greater than the minimum measured berm length (13 m). Considering that measured lengths of the referenced berms had some uncertainty, a length filter value of 17 m was reasonable.

The orientation filter was mainly used to distinguish earthen berms from land surface irregularities near channel banks. With the exception of channel bank protection berms, earthen berms on rangelands are generally oriented perpendicular to the general flow direction to intercept runoff. By using an orientation filter, objects with small orientation angles compared to the general flow direction (in other words, objects that are more parallel to the general flow direction) were removed. In our study, the general flow direction at the three study sites was from west to east, and toward Altar Wash, therefore we defined west to east as the referenced flow direction. In the case of identifying berms in other research sites that have different general flow direction (for example, from north to south), the most recommended way is to rotate the images (*Z1_MGR* or *Z1_GEO*) with certain angle to make the general flow direction from west to east. This is because angle calculation is usually considered X-axis that from west to east as a referenced axis.

As stated in the method section, we directly set orientation threshold to $|\theta|$, which is the orientation angle between an identified object and the referenced flow direction, rather than to $|\theta \pm \beta|$, which is the orientation angle between each identified object and its corresponding upslope local flow direction. When compared to Sites A and B, the true channel flow direction at Site C had greater orientation angle, β, as compared to the west-east referenced direction. As a result, the orientation threshold for Site C was adjusted from 21 to 25°, such that the $|\theta \pm \beta|$value at Site C was relatively similar to those at Sites A and B. The implication here is that if the true channel flow direction deviates more from the general flow direction (for example, in our study from west to east) the orientation filter threshold will increase.

Because deeply incised channels introduce greater variability and result in many false-positive objects, it might seem reasonable to use a buffer to remove these channels from the topographic data. However, a simple buffer around the channels proved to be inadequate. Identifying the channel network and subsequently buffering the network to maximize noise reduction while also preserving berm features was difficult. Additional efforts are needed to extract the channel network and considerable extraction uncertainty may still remain even when using a terrain attribute threshold rather than a contributing area threshold (Clubb et al., 2014). Furthermore, the buffer width should vary according to the width of each channel segment, otherwise a wide buffer would remove true berms located near to narrow channel segments. However, channel width is often difficult to determine from DEMs.

The eccentricity threshold was used to find linear objects. Among the 53 referenced berms at Site A, 50 berms (94%) had an eccentricity greater than 0.95, which was the basis to optimize eccentricity threshold. Values ranging from 0.90 to 0.95 with an increment of 0.1 were tested for optimizing the eccentricity filter. The optimized eccentricity threshold could be directly applied to Site B with high identification accuracy, however, was adjusted from 0.95 to 0.93 for Site C. In contrast to Sites A and B, many of the earthen berms at Site C were constructed with earthen spurs perpendicular to the main berm to which the spurs were attached, thus decreasing the general object eccentricity (refer to Fig. 6). The use of the eccentricity threshold could be expanded upon to identify berms that have a more curved or non-linear general shape. As we noted in the Results section, if we set the eccentricity threshold to a value of 0.75 or less, circular stock tank berms were preserved in the identification results. Therefore, one could use the eccentricity filter to identify curved berms or other more circular features such as tanks and ponds by removing objects that have eccentricity greater than 0.75.

The analysis of vertical profiles of objects was used to confirm whether the objects identified through use of horizontal filters followed the characteristic cross-sectional shape of a typical berm. The main role of the vertical profile analysis was to reduce the number of false-positive objects (Tables 1–6). In other words, analyzing vertical profiles does not increase the detection rate, but the precision rate.

4.4. Implications and limitations of the proposed workflows

The orientation and eccentricity filters were optimized using information from those reference berms that shared the dominant orientation and eccentricity. This resulted in a small proportion of true berms being removed when the filters are applied. This was a compromise that substantially reduced the rate of false detections, but also explains why detection rates of 100% were not achieved. These workflows apply to 1-m DEM datasets alone. However, future development of a method to fuse aerial imagery, 3D hillshade representations, and DEMs can be expected to improve berm detection results.

The workflows automatically and successfully extracted several dozen objects from a DEM consisting of millions of pixels; if this output was followed by manual inspection, false-positive objects could be removed with minimal effort. Manual investigations of false-positive objects (FPs) at the three sites showed that those FPs were either bank protection berms, earthen spurs, or random surface irregularities, and not water spreader berms. Differentiating those false-positive objects from water spreader berms solely based on the topographic data was not obvious, because they were similarly linear with relatively high elevations as compared to the immediate surrounding area. However, with the aid of aerial imagery and 3D hillshade representations, these false-positive objects could be easily filtered out by manual inspection.

5. Conclusion

This study describes two workflows to semi-automatically detect linear earthen water spread berms in the Altar Valley, Arizona, southwestern US, using high-resolution topographic data. Initial identification was conducted using either morphological grayscale reconstruction (MGR) or the Geomorphon (GEO) method, followed by refinements through geometrically based filters and a vertical profile analysis. One site was used to optimize thresholds and parameters of the workflows which were then validated at two additional sites. Based on the identification results, the following conclusions can be drawn.

(1) Both of the workflows can successfully identify the majority of the earthen berms; the MGR method could produce final precision and detection rates of up to 92% and 75%, respectively. Manual inspection of the semi-automated workflow outputs can further refine results to remove false-positives. These results suggest that identifying isolated, irregularly distributed, and relatively small earthen berms using available high-resolution topographic data is feasible.
(2) Detection rate and precision rate were improved by assessing object shape and cross-sectional characteristics. Length, orientation angle, and eccentricity are important parameters for identifying true earthen berms. However, the eccentricity and orientation filter threshold were not constant values across the three sites and require adjustment according to the unique channel flow direction and berm shapes of a particular study site and general landscape.
(3) The MGR-based workflow yielded better identification accuracy than did the GEO-based workflow, because for the GEO method, only those pixels classified as “summit” were used to identify potential earth berms and the pixel classification is affected by the lookup distance and flatness parameters. Testing and utilizing additional Geomorphon output/input parameters might improve the detection results.

References

Arefi, H., & Hahn, M. (2012). A morphological reconstruction algorithm for separating off-terrain points from terrain points in laser scanning data. *The International Archives of the Photogrammetry, Remote Sensing and Spatial Information Sciences, 36*.

Cazorzi, F., Fontana, G. D., Luca, A. De, Sofia, G., & Tarolli, P. (2013). Drainage network detection and assessment of network storage capacity in agrarian landscape. *Hydrological Processes, 27*, 541–553. https://doi.org/10.1002/hyp.9224

Clubb, F. J., Mudd, S. M., Milodowski, D. T., Hurst, M. D., & Slater, L. J. (2014). Objective extraction of channel heads from high-resolution topographic data. *Water Resources Research, 50*, 4283–4304. https://doi.org/10.1002/2013WR015167

Conrad, O., Bechtel, B., Bock, M., Dietrich, H., Fischer, E., Gerlitz, L., Wehberg, J., Wichmann, V., & Boehner, J. (2015). System for automated geoscientific analyses (SAGA) v. 2.1.4. Geosci. *Model Dev, 8*, 1991–2007. https://doi.org/10.5194/gmd-8-1991-2015

Deng, C., Zhang, G., Liu, Y., Nie, X., Li, Z., Liu, J., & Zhu, D. (2021). Advantages and disadvantages of terracing: A comprehensive review. *Int. Soil Water Conserv. Res., 9*, 344–359. https://doi.org/10.1016/j.iswcr.2021.03.002

Dettenmaier, S. J., Messmer, T. A., Hovick, T. J., & Dahlgren, D. K. (2017). Effects of livestock grazing on rangeland biodiversity: A meta-analysis of grouse populations. *Ecology and Evolution, 7*, 7620–7627. https://doi.org/10.1002/ece3.3287

GRASS Development Team. (2017). *Geographic resources analysis support system (GRASS) software, version 7.2*. Open Source Geospatial Foundation. Electronic document. http://grass.osgeo.org.

Havstad, K., Peters, D., Allen-Diaz, B., Bartolome, J., Bestelmeyer, B., Briske, D., Brown, J., Brunson, M., Herrick, J., Huntsinger, L., Johnson, P., Joyce, L., Pieper, R., Svejcar, T., & Yao, J. (2015). *The western United States rangelands: A major resource*. https://doi.org/10.2134/2009.grassland.c5

Jasiewicz, J., & Stepinski, T. F. (2013). Geomorphons — a pattern recognition approach to classification and mapping of landforms. *Geomorphology, 182*, 147–156. https://doi.org/10.1016/j.geomorph.2012.11.005

McKean, J., & Roering, J. (2004). Objective landslide detection and surface morphology mapping using high-resolution airborne laser altimetry. *Geomorphology, 57*, 331–351. https://doi.org/10.1016/S0169-555X(03)00164-8

Nichols, M. H., & Degginger, T. (2021). The landscape impact of unmaintained rangeland water control structures in southern Arizona. USA *Catena, 201*. https://doi.org/10.1016/j.catena.2021.105201.

Nichols, M. H., Magirl, C., Sayre, N. F., & Shaw, J. R. (2018). The geomorphic legacy of water and erosion control structures in a semiarid rangeland watershed. *Earth Surface Processes and Landforms, 43*, 909–918. https://doi.org/10.1002/esp.4287

Nichols, M. H., Shaw, J. R., & Brandau, W. K. (2021). Unintended consequences of rangeland conservation structures. *Int. Soil Water Conserv. Res., 9*, 158–165. https://doi.org/10.1016/j.iswcr.2020.11.006

Peterson, H. V., & Branson, F. A. (1962). Effects of land treatments on erosion and vegetation on range lands in parts of Arizona and New Mexico. *Journal of Range Management, 15*, 220. https://doi.org/10.2307/3895254

Polyakov, V. O., Nichols, M. H., McClaran, M. P., & Nearing, M. A. (2014). Effect of check dams on runoff, sediment yield, and retention on small semiarid watersheds. *Journal of Soil and Water Conservation, 69*, 414–421. https://doi.org/10.2489/jswc.69.5.414

Sărășan, A., Józsa, E., Ardelean, A. C., & Drăguț, L. (2019). Sensitivity of geomorphons to mapping specific landforms from a digital elevation model: A case study of drumlins. *Area, 51*, 257–267. https://doi.org/10.1111/area.12451

Schwanghart, W., & Kuhn, N. J. (2010). TopoToolbox: A set of matlab functions for topographic analysis. *Environmental Modelling & Software, 25*, 770–781. https://doi.org/10.1016/j.envsoft.2009.12.002

Stavi, I., Gusarov, Y., & Halbac-Cotoara-Zamfir, R. (2019). Collapse and failure of ancient agricultural stone terraces: On-site geomorphic processes, pedogenic mechanisms, and soil quality. *Geoderma, 344*, 144–152. https://doi.org/10.1016/j.geoderma.2019.03.007

Stavi, I., Rozenberg, T., Al-Ashhab, A., Argaman, E., & Groner, E. (2018). Failure and collapse of ancient agricultural stone terraces: On-site effects on soil and vegetation. *Water, 10*, 1400. https://doi.org/10.3390/w10101400

Stavi, I., Siad, S. M., Kyriazopoulos, A. P., & Halbac-Cotoara-Zamfir, R. (2020). Water runoff harvesting systems for restoration of degraded rangelands: A review of challenges and opportunities. *Journal of Environmental Management, 255*, Article 109823. https://doi.org/10.1016/j.jenvman.2019.109823

Steinfeld, C. M. M., Kingsford, R. T., & Laffan, S. W. (2013). Semi-automated GIS techniques for detecting floodplain earthworks. *Hydrological Processes, 27*, 579–591. https://doi.org/10.1002/hyp.9244

Tarolli, P. (2014). High-resolution topography for understanding Earth surface processes: Opportunities and challenges. *Geomorphology, 216*, 295–312. https://doi.org/10.1016/j.geomorph.2014.03.008

Tarolli, P., Sofia, G., & Dalla Fontana, G. (2012). Geomorphic features extraction from high-resolution topography: Landslide crowns and bank erosion. *Natural Hazards, 61*, 65–83. https://doi.org/10.1007/s11069-010-9695-2

Tucker, G. E., Catani, F., Rinaldo, A., & Bras, R. L. (2001). Statistical analysis of drainage density from digital terrain data. *Geomorphology, 36*, 187–202. https://doi.org/10.1016/S0169-555X(00)00056-8

Vincent, L. (1993). Morphological grayscale reconstruction in image analysis: Applications and efficient algorithms. *IEEE Transactions on Image Processing, 2*, 176–201. https://doi.org/10.1109/83.217222